Regional Gene Expression in the Retina, Optic Nerve Head, and Optic Nerve of Mice with Experimental Glaucoma and Optic Nerve Crush

Casey J. Keuthan[1*], Julie Schaub[1], Meihan Wei[2], Weixiang Fang[2], Sarah Quillen[1], Elizabeth Kimball[1], Thomas V. Johnson[1], Hongkai Ji[2], Donald J. Zack[3], and Harry A. Quigley[1]

[1]Department of Ophthalmology, Wilmer Eye Institute, Johns Hopkins University School of Medicine, Baltimore, MD 21231, USA

[2]Department of Biostatistics, Johns Hopkins University Bloomberg School of Public Health, Baltimore, MD 21205, USA

[3]Departments of Ophthalmology, Wilmer Eye Institute, Neuroscience, Molecular Biology and Genetics, and Genetic Medicine, Johns Hopkins University School of Medicine, Baltimore, MD 21231, USA

[*]Corresponding Author: Casey J. Keuthan (ckeutha1@jh.edu)

Abstract

A major risk factor for glaucomatous optic neuropathy is the level of intraocular pressure (IOP), which can lead to retinal ganglion cell axon injury and cell death. The optic nerve has a rostral unmyelinated portion at the optic nerve head followed by a caudal myelinated region. The unmyelinated region is differentially susceptible to IOP-induced damage in rodent models and in human glaucoma. While several studies have analyzed gene expression changes in the mouse optic nerve following optic nerve injury, few were designed to consider the regional gene expression differences that exist between these distinct areas. We performed bulk RNA-sequencing on the retina and on separately micro-dissected unmyelinated and myelinated optic nerve regions from naïve C57BL/6 mice, mice after optic nerve crush, and mice with microbead-induced experimental glaucoma (total = 36). Gene expression patterns in the naïve unmyelinated optic nerve showed significant enrichment of the Wnt, Hippo, PI3K-Akt, and transforming growth factor β pathways, as well as extracellular matrix–receptor and cell membrane signaling pathways, compared to the myelinated optic nerve and retina. Gene expression changes induced by both injuries were more extensive in the myelinated optic nerve than the unmyelinated region, and greater after nerve crush than glaucoma. Changes three and fourteen days after injury largely subsided by six weeks. Gene markers of reactive astrocytes did not consistently differ between injury states. Overall, the transcriptomic phenotype of the mouse unmyelinated optic nerve was significantly different from immediately adjacent tissues, likely dominated by expression in astrocytes, whose junctional complexes are inherently important in responding to IOP elevation.

Keywords

gene expression, transcriptomics, optic nerve, retina, glaucoma, mouse, nerve crush

39 **Introduction**

40 Glaucoma is the second leading cause of blindness worldwide [1], and causes vision loss by
41 killing retinal ganglion cells (RGCs). One of the most prominent risk factors for glaucomatous optic
42 neuropathy is the level of intraocular pressure (IOP) [1]. Elevated IOP in rodent models produces optic
43 nerve (ON) pathology that is first observable at the unmyelinated segment of the optic nerve head
44 (ONH), the zone corresponding to the site of injury in human glaucoma, the lamina cribrosa [2-4].
45 Rodent glaucoma models provide the opportunity to study axonal and astrocytic responses in the
46 laboratory over short time frames. The dominant glial cell of the ONH in all mammals is the astrocyte,
47 though some microglia are also present. Astrocytes reside on connective tissue beams that course
48 across the primate and human ONH. In the much smaller corresponding area of the mouse (the
49 unmyelinated optic nerve [UON]), there is minimal connective tissue and astrocytes bridge from one
50 side to the other of the ONH to form a so-called "glial lamina" [5, 6].

51 ONH astrocytes have distinct properties compared to most other astrocytes, even differing in
52 important features from astrocytes in the retina and distal ON, exhibiting features not previously
53 recognized [7]. They serve the biomechanical function of resisting IOP-generated stress by virtue of
54 connections to the ONH perimeter through integrin-linked transmembrane junctions to their basement
55 membrane. They have specialized junctional complexes on the internal cell membrane facing their
56 basement membrane in both mouse and human ONH [8, 9]. Transcriptomic studies have now revealed
57 many regional phenotypes in brain astrocytes [10]. The ONH astrocyte is likely to exhibit unique gene
58 expression patterns since it is potentially the only astrocyte that is subjected to differential stress across
59 the cell from its connection to the basement membrane and from the trans-ONH pressure differential
60 from inside to outside the eye. However, the local gene expression of UON astrocytes has only recently
61 been studied in the naïve state [11] and has not been studied in disease states.

62 There have been investigations of gene expression changes in the retina and the ON in various
63 injury models such as microbead-induced glaucoma and ON crush in rodents and cultured astrocyte
64 models [12-18]. Yet, the majority of this research did not distinguish the rodent UON from that of the
65 myelinated optic nerve (MON) region and other nearby tissues [15, 19, 20]. Moreover, conflicting
66 reports between whole ONH tissue studies and cultured astrocytes further confound accurate definition
67 of the gene expression changes occurring in these cells [12, 21, 22].

68 We performed bulk RNA-sequencing (RNA-seq) on the retina and micro-dissected UON and
69 MON to characterize the region-specific transcriptome of mouse eyes in the naïve state and following
70 ON crush and experimental ocular hypertension. We identified unique gene profiles of each tissue
71 region, and found genes related to the interaction between extracellular matrix and cell membrane
72 receptors, along with several downstream pathways important in integrin-linked signaling, significantly
73 enriched in the naïve UON. Interestingly, we found that the gene changes in MON were more extensive
74 than the UON in both IOP elevation and crush models, and these changes occurred in a time-dependent
75 manner. There were increases in both putative beneficial and detrimental astrocytic markers in both
76 models.

77

78 **Results**

79 ***Distinct expression patterns in naïve UON, MON, and retinal tissues***

80 Total RNA was extracted from micro-dissected UON, MON, and whole retina of four B6 naïve
81 mice (2 male and 2 female mice per group) and pooled by sex for library preparation and RNA-seq
82 (Figure 1A). Replicates of each tissue type clustered well by principal component analysis (PCA; Figure
83 1B), demonstrating established markers for ON and retina in each group (Figure 1C). We also compared
84 expression of several genes known to be typically expressed by astrocytes, oligodendrocytes, microglia,

85 and capillaries in each tissue group (Figure 1C). We next compared these transcriptomic data with qPCR
86 data from a separate cohort of naïve mice for a series of genes known to be expressed in astrocytes and
87 often associated with beneficial or detrimental phenotypes in these glia and other genes of interest
88 (Figure 1D and Figure S1). Overall, the regional expression differences of these genes were similar
89 between RNA-seq and qPCR.

90 Differential expression analysis was performed to extract regional gene signatures of UON and
91 MON. For this, we identified subsets of genes that were significantly upregulated in UON and MON
92 compared to the other two tissue types (Figure 2A). There were 12686 genes commonly upregulated
93 (from both pairwise comparisons) in UON and 868 genes significantly enriched in MON (Figure 2A).
94 KEGG analysis of significantly enriched UON genes compared to MON and retina tissue included
95 pathways known to be associated with astrocyte functions in this region: extracellular matrix–receptor
96 interactions, focal and cell adhesion, and transforming growth factor β (TGFβ) signaling pathways
97 (Figure 2B-C). In MON, pathway analysis of upregulated genes using the KEGG database collection
98 showed enrichment of steroid biosynthesis and axon guidance pathways in MON upregulated genes
99 (Figure 2B-C and E). The differentially expressed genes (DEGs) in UON coding for molecules in the
100 critical pathway of cell attachment to the extracellular matrix (Figure 2C) included transmembrane
101 molecules (e.g. integrins: α3,5,8 and β1,4, syndecan, and dystroglycan), basement membrane
102 components (e.g. collagen 4 and laminins α4; β1,2; γ2), and extracellular matrix members near the
103 cellular attachment zone (e.g. fibronectin, tenascin, and perlecan). Similar analysis of the naïve retinal
104 tissue found enrichment of neuronal/photoreceptor-related pathways, as expected (Figure S2).

105 We specifically compared gene expression between the two ON regions and found 1646 genes
106 enriched in UON and 1522 enriched genes in MON (Figure 2D). Similar KEGG pathways were enriched
107 from these UON genes compared to our earlier analysis in which UON and MON were contrasted with
108 retinal tissue (Figure 2E). The KEGG pathways selectively enriched in MON were more often related to

109 axonal functions (e.g., steroid biosynthesis and glutamatergic synapse), though axonal guidance was an
110 area seen in both UON and MON analyses (Figure 2E).

111 ***Differential gene expression after ON crush injury***

112 We performed RNA-seq on the retina, UON, and MON following ON crush injury (Figure 3A). For
113 this study, we examined two time points, three days (early, 3D) and two weeks (late, 2W) after crush,
114 with a similar pooling strategy as used in the naïve tissue samples (Figure 3A). We estimated the degree
115 of injury or loss of RGCs by looking at the expression of several genes prominently expressed in RGCs in
116 the retinal tissue samples (Figure S3). Many of these RGC marker genes were significantly reduced by
117 three days after crush, including *Rbpms*, *Rbpms2*, and *Sncg* (Figure S3). At two weeks after crush, when
118 most RGC loss would typically have occurred after crush injury, RGC gene expression was drastically
119 downregulated (by greater than nine-fold for most genes) compared to naïve control retinas, suggesting
120 substantial RGC loss following optic crush injury (Figure S3).

121 We compared DEGs at early and late crush time points between UON, MON, and retinal tissue
122 (Figure 3 A-B). Samples from the same tissue region clustered together by PCA, with some separation
123 between crush time points within each region (Figure 3B). Gene expression changes in the retina
124 differed the most from the ON tissue regions (Figure 3C). In total, our RNA-seq analysis revealed 136 and
125 349 DEGs in the retina at early and late ON crush time points, respectively (Figure 3C and Spreadsheet
126 S5). DEGs three days after crush mostly consisted of genes involved in the response to a stimulus/insult,
127 whereas gene expression changes two weeks after crush also included genes related to neuronal cell
128 death and synaptic functions (Figure S6).

129 At three days, DEGs shared by all tissue regions included *Egr1* (early growth response 1, *Ccn1*
130 (cellular communication network factor 1), and *Serpina3n* (serine (or cysteine) peptidase inhibitor, clade
131 A, member 3N), which were upregulated with injury (Spreadsheet S1). Notably, while *Knstrn*

132 (kinectochore-localized astrin/SPAG5 binding) was significantly changed in all tissues three days after
133 crush, this gene was upregulated in both UON and MON but downregulated in the retinal tissue
134 (Spreadsheet S1). Overall, UON and MON had 146 and 188 DEGs in common at three days and two
135 weeks after crush, respectively (Figure 3C and Spreadsheet S1). Of these, all but the non-protein coding
136 gene *Neat1* (nuclear paraspeckle assembly transcript 1) followed a similar expression pattern between
137 the two tissues at three days after crush (Spreadsheet S1). The number of shared genes by all three
138 tissue regions increased two weeks after crush (Figure 3C). These 27 genes followed the same
139 expression pattern (either upregulated or downregulated) except for *A2m* (alpha-2-macroglobulin), a
140 reactive astrocyte marker, which was uniquely downregulated in UON at this time point (Figure 3D and
141 Spreadsheet S1). Interestingly, eight genes had opposite expression changes two weeks after crush:
142 *Col2a1*, *Trim56*, *Cnn1*, *Gp1bb*, *Bub1*, *Slc39a14*, *Oas3*, and *Nhlrc3* (Spreadsheet S1).

143 Gene expression changes were greater in MON compared to UON and retina at both crush time
144 points (Figure 3C). The 2368 DEGs in the MON at three-day crush were associated with pathways that
145 included processes like cell cycle and cytokine signaling (Figure 3D). Over 40% (n = 977) of these genes
146 were also differentially expressed at the two week crush time point (Figure 3E and Spreadsheet S4).
147 While most MON DEGs exhibited prolonged changes (either upregulated or downregulated at both time
148 points), several genes displayed an opposing response between early and late crush time points (Figure
149 3H). *Dlk1* (delta like non-canonical Notch ligand 1), *Gpd1* (glycerol -3-phosphate dehydrogenase 1
150 (soluble)), and *Il3ra* (interleukin 31 receptor A) were significantly upregulated at three days after crush
151 but significantly downregulated at the two week time point (Figure 3H and Spreadsheet S4). Conversely,
152 seven genes were initially downregulated, but substantially increased later following crush (Figure 3H
153 and Spreadsheet S4). DEG analysis of two week crush samples yielded 1693 significantly changed genes
154 in the MON (Figure 3E and F). While pathways such as phagocytosis and NF-kappa beta signaling were
155 still among the enriched KEGG pathways at two weeks, other processes like extracellular matrix–

156 receptor interactions and complement and coagulation cascades were also significantly upregulated
157 (Figure 3D).

158 There was a weaker response to crush in the UON (as compared to MON) (Figure 3C and F).
159 Notably, these UON genes were largely different between crush time points. Of the 210 UON DEGs at
160 three days, only 25.7% were significantly changed at both time points (Figure 3E and Spreadsheet S3).
161 Like the crushed MON tissue, these common genes showed consistent expression at both time points
162 except for *Ccnf* (cyclin F) and *Bub1* (BUB1, mitotic checkpoint serine/threonine kinase) (Figure 3G and
163 Spreadsheet S3). Generally, UON expression changes early after crush were in upregulated genes
164 involved in cell cycle regulation and cell division (Figure 3D and E). Despite 501 DEGs observed in the
165 UON at two weeks crush, these genes were not associated with specific KEGG pathways, aside from an
166 enrichment in apoptosis (Figure 3D). Taken together, these data suggest that there is a differential
167 response to crush within ON tissue regions.

168 ***Differential gene expression in the glaucoma model***

169 The injection of microbeads into the anterior chamber produces IOP elevation known to cause
170 RGC death that is maximal by 6 weeks [23] (Figure 4A, Figure S4, Table S1). Mice exposed to elevated
171 IOP followed prior experience with bead injection [23, 24], having significant mean IOP elevation at
172 three days, decreasing at two weeks and with minimal difference from baseline at six weeks (Figure S4,
173 Table S1). Micro-dissected UON, MON, and retinal tissue was collected at three days (early, 3D), two
174 weeks (middle, 2W), and six weeks (late, 6W) post-injection to characterize gene expression changes
175 spanning the time course of this model (Figure 4A). There was a clear upregulation of
176 inflammatory/immune response genes in the retina detectable at the earliest glaucoma time point,
177 including *Gfap*, *Osmr*, *Fgf2*, *Edn2*, *Stat3*, and *Socs3* (Figure S6B). This stress response was generally
178 sustained in the retina through at least two weeks after IOP elevation before falling back to baseline

179 expression levels (Figure S6B). We estimated the degree of RGC injury from the retinal expression of
180 RGC genes in the glaucoma retinal tissue, as was carried out in the crush samples. There was an
181 immediate reduction in expression at three days in several RGC-specific genes, including *Rbpms* and
182 *Tubb3*, that remained similarly downregulated at six weeks (Figure S3).

183 PCA showed a clear separation of samples by tissue region (Figure 4B). As in crush injury, gene
184 expression changes differed greatly between UON, MON, and retina (Figure 4B). At three days, only
185 three genes were significantly upregulated in all regions: 1) *Timp1* (tissue inhibitor of
186 metalloproteinase), 2) *Fgcr* (Fc receptor, IgG, low affinity III); and 3) *Cd68* (CD68 antigen) (Spreadsheet
187 S2). Yet, the expression patterns of these genes varied greatly between tissue regions across later time
188 points, where upregulation in the retina typically persisted longer than increased expression in the ON
189 tissues (Spreadsheet S2). Few to no DEGs were common at the later glaucoma time points (Figure 4C
190 and Spreadsheet S2). An additional 28 genes were commonly upregulated in UON and MON regions at
191 the early time point but only four DEGs (*Fcrls*, *Pla2g3*, *Olig2*, and *Tsc22d3*) were shared by two weeks
192 (Figure 4C and Spreadsheet S2).

193 Similar to ON crush, the number of DEGs at the three day and two week time points were
194 greatest in MON (n = 427 at three days, n = 493 at two weeks) and fewest in UON tissues (n = 129 at
195 three days, n = 69 at two weeks) (Figure 4C). Early response genes in the UON were primarily
196 upregulated and related to cell proliferation pathways (Figure 4D and F). One noteworthy pathway
197 upregulated in both UON and MON glaucoma at three days was the p53 pathway, which was also
198 increased in UON and MON three days after crush injury (Figure 3D and 4D). In addition to the cell cycle-
199 related pathways shared with UON three days after microbead injection, top MON responses also
200 included phagocytosis and cytokine-cytokine receptor interactions (Figure 4D). At two weeks, many
201 stress response pathways like P13K-Akt and JAK-STAT signaling were also enriched among the MON
202 genes (Figure 4D).

203 Although gene expression changes were far more subtle in the glaucoma model, UON and MON
204 DEGs compared to naïve tissue still varied between each of the three time points akin to crush (Figure
205 4E). Only 14 DEGs were shared between the three day and two week time points in UON; by six weeks,
206 only four of these genes were significantly upregulated (Figure 4E and Spreadsheet S3). In the MON,
207 there was a robust response to IOP elevation that persisted through two weeks and few changes by six
208 weeks (Figure 4E-F). Only 18 MON DEGs were consistently changed among the three time points, and
209 131 genes that had a sustained response (either upregulated or downregulated) through two weeks
210 (Figure 4E and Spreadsheet S4). Of these, response to stimulus and several integrin subunits were
211 significantly elevated (Spreadsheet S4).

212 ***Injury-specific responses in ON tissue regions***

213 We compared our ON crush and glaucoma RNA-seq datasets to determine whether there are
214 gene expression changes in the different ON tissue regions that are unique to the glaucoma disease
215 model. While 56% of glaucoma DEGs from our UON analysis (n = 112 out of 200 total DEGs) were
216 uniquely changed in at least one of the glaucoma time points (Figure 5A), individual inspection of these
217 genes showed many still elevated or reduced in ON crush (Figure 5B and Spreadsheet S6). In these
218 cases, the genes did not meet our preset threshold for statistical significance in our crush analysis to be
219 included as a DEG in the crush dataset. Of the 88 common DEGs between crush and glaucoma samples
220 in the UON, we found a small subset, such as *Cks2*, that had uniquely significant expression patterns
221 between the models (Figure 5B and Spreadsheet S6).

222 There were proportionally fewer unique DEGs in MON glaucoma samples compared to ON crush
223 (22.2%, n = 105 out of 472 total DEGs) (Figure 5A). However, these differences in response were more
224 apparent on the individual gene level than in UON, particularly in high-expressing DEGs (Figure 5B and
225 Spreadsheet S6). Interestingly, there were minimal examples of inversely shared gene expression among

226 the 367 MON DEGs (Spreadsheet S6). Overall, these data suggest that much of injury response at the
227 gene level is shared by the ON crush and ocular hypertensive injury models.

228 ***Astrocyte responses to ON injury***

229 We examined our RNA-seq datasets for genes that are reported to be associated with either
230 general (or PAN) astrocyte behavior (e.g., *Gfap, Ptx3*), detrimental (or A1-specific) astrocyte/microglial
231 responses (e.g., *C3, Serping1, C1qa, Il1a*) or beneficial (or A2-specific) astrocyte/microglial responses
232 (e.g., *Stat3, Sphk1*) (Figure 5D). Astrocyte gene responses between crush and glaucoma samples were
233 generally consistent (Figure 5D). There was no clear A1 or A2-specific phenotype in UON samples or
234 retinal samples with ON injury (Figure 5D and Figure S7). MON had more consistently higher expression
235 of some A2 astrocyte markers (e.g., *Ptgs2, Slc10a6, B3gnt5*) in early crush and glaucoma time points that
236 shifted to an upregulation of A1-specific (detrimental) markers (e.g., *Serping1*, *C3*, *Fbln5*) after two
237 weeks; however, neither an A1 nor A2 phenotype dominated in our time course of ON injury samples
238 (Figure 5D).

239

240 **Discussion**

241 There have been several previous studies of gene expression in the ON of mouse or rat. In some
242 of these, the UON segment was specifically dissected from the MON [13, 14]. In most studies, there was
243 inclusion of MON, preONH tissue, or retina [15-18]. In the present study, we compared the gene
244 expression in retina, UON, and MON by microdissection, demonstrating that these areas have
245 dramatically different expression patterns that indicate regional phenotypes in both the naïve and
246 diseased states. In part, this would be expected from the morphological differences in astrocytes of the
247 two regions [25]. A recent report by Mazumder et al. also investigated regional astrocyte gene
248 expression in the mouse unmyelinated ONH (equivalent to UON in our studies) using the ribotag

249 approach, which enriches for translated mRNAs [11]. While this and the present study had certain
250 overlapping or complementary findings, there were also significant differences. For example, in naïve
251 UON alone, *Cartpt* is prominently expressed in both datasets and in our disease models, *Cartpt* is
252 significantly downregulated. On the other hand, some of the enriched pathways differed between the
253 two datasets. Notably, only in our study was cell—extracellular matrix interaction pathways so
254 prominently enriched in the UON region. Further, the UON astrocytes in Mazumder et al.'s report found
255 many genes typical for photoreceptors were expressed within the UON ribosomal mRNA, which we did
256 not. Potential methodological differences could explain these disparities. Astrocytes of the retina and
257 the ON derive from different embryologic origins; retinal astrocytes arise from an optic disc progenitor
258 zone driven by transcription factor *Pax2*, while ON astrocytes derive from progenitors in the optic stalk
259 [26]. Among many differences between the two types, retinal astrocytes are uniformly spaced (tile-like),
260 while UON astrocytes have overlapping processes that bridge from one side of the ONH to the other [5].
261 Thus, it is not surprising, but still intriguing that expression patterns of the adjacent UON and MON are
262 so different.

263 The major pathways identified in naïve UON, a tissue in which the vast majority of cells are
264 astrocytes, matched known features of the normal anatomy/function of the UON, whose role in
265 adherence to surrounding connective tissue vitally resists the biomechanical stress generated by IOP. It
266 is noteworthy that the UON tissue exhibited higher expression of genes related to interactions between
267 cells and the extracellular matrix, focal and intercellular adhesion, and four other signaling pathways:
268 Hippo, Wnt, PI3K-Akt, and TGFβ. By contrast, the enriched MON genes represented important pathways
269 for insulin, Ras, sphingolipid, and ErbB signaling. An important pathway in common between UON and
270 MON in our analysis was axon guidance. In the mouse UON, the vast majority of cells locally generating
271 RNA are astrocytes [24]. The major cellular content difference between UON and MON is the presence
272 of oligodendrocytes in the latter region. Thus, the observed DEG differences are understandable, but

273 indicate that cell to matrix adhesion is not as prominent in the MON. While the MON must withstand
274 some motion in the orbit, it is not subjected to the stress generated by IOP. We have recently
275 demonstrated that UON astrocytes and astrocytes of all mammalian ONH lack aquaporin expression
276 [27], and differential *Aqp4* expression was also observed in the current study (data not shown). It is now
277 widely recognized that astrocyte genetic expression varies substantially in the many regions of the
278 central nervous system [28, 29]. The regional phenotype of UON astrocytes is clearly focused on
279 interactions between these cells and their extracellular environment, a process mediating
280 mechanosensation and mechanotranslation. Recent studies of regional gene expression by brain
281 astrocytes found none of the highly expressed pathways involved transmembrane signaling to
282 extracellular matrix described here, illustrating the uniqueness of astrocytes in the UON [30].

283 One pathway identified as upregulated in both UON and MON in early glaucoma and crush time
284 points was the p53 pathway. Actions attributed to this widely studied pathway include control of cell
285 division and activation of caspase-mediated apoptosis[31-33]. Interestingly, cell cycle genes that were
286 upregulated in both UON and MON were *Cdk1*, *Ccnb1*, *Ccnb2* and *Top2a*, suggesting increased cell
287 division. At the same time, inhibitors of p53 activity were also upregulated (*Cdkn3* and *Gtse*). In MON,
288 but not UON, further downstream partners of p53 that were upregulated included *Serpine1* and *Thbs1*,
289 suggesting an effect of inhibiting angiogenesis. One genome wide association study found a relation
290 between a p53 polymorphism and one human glaucoma phenotype[34], while another found KEGG
291 pathways associated with human open angle glaucoma were focal adhesion, and Wnt and TGFβ
292 signaling, strikingly similar to the naïve UON pathways active in our study [35].

293 The gene expression changes in the UON with glaucoma differ from those of the MON in
294 glaucoma, with greater numbers of genes differentially expressed in MON. The MON had more
295 increases in cell cycle genes. Both astrocytes and microglia proliferate in the mouse glaucoma model
296 [24]. In both mouse and rat ocular hypertension models, there was loss of oligodendrocytes in the MON

297 and oligodendrocyte precursor cells proliferated, while activation of microglia was detected only in
298 advanced damage nerves [36]. We found that upstream stimulators of Aurora proliferative signaling had
299 increased expression in UON after three-day glaucoma (*Cenpa*, *Arhgef*, *Dlgap4*). However, molecules
300 involved in cell cycling can be inhibitory (e.g., p53 or *Tp53*), as well as stimulating to proliferation. We
301 found that *Cdk1* (cyclin-dependent kinase 1) was increased in UON and MON at three day ON crush and
302 glaucoma tissues, though cyclin D1 (*Ccnd1*), its downstream target was not. On the other hand, *Cdkn2c*
303 (cyclin-dependent kinase inhibitor 2c) was upregulated in the UON at the three day crush time point and
304 *Cdkn3* (cyclin-dependent kinase inhibitor 3), which prevents the activation of *Cdk2*, was also increased in
305 early glaucoma in this same region. These molecules would tend to inhibit proliferation. Interestingly,
306 genome wide association studies have identified *CDKN2b* polymorphisms as associated with either
307 increased or decreased risk of open angle glaucoma [18]. *Lockd* gene was increased in both three day
308 and two week UON glaucoma and three day UON crush. Its action enhances *Cdkn1b* transcription,
309 potentially acting as another cell cycle inhibiting factor [37].

310 There are some similarities between our findings and those of Morrison et al. using a glaucoma
311 model in whole rat ON, which found increased extracellular matrix and TGFβ1 gene, as well as
312 upregulation of cell cycle genes [14, 15]. These studies included both UON and MON together in the
313 analysis, as did DEG studies in mouse after nerve crush by Qu and Jakobs [13]. Howell et al. studied
314 DBA/2J glaucoma mouse gene expression in specimens that included some retinal tissue, choroid and
315 sclera, and an unknown amount of MON [38]. Upregulated pathways included the immune response,
316 chemotaxis, and cell–matrix interaction, including tenascin C, integrins, fibronectin, Timp 1 and 2, and
317 several collagens. Several of these individual genes were significantly upregulated in our two disease
318 models. Our demonstration that there are substantial differences in gene expression between retina
319 and MON compared to UON suggests selective dissection of these tissues is important in future studies.

320 There were both shared and unique gene expression differences between the glaucoma and
321 nerve crush models. The number of genes that significantly increased was greater in the MON compared
322 to the UON in both injury models, despite the fact that the axon injury is known to be initiated in the
323 UON in glaucoma while the crush injury is applied directly to the MON [3]. This observation makes it
324 more likely greater differential gene expression in MON is not simply related to the addition of
325 oligodendrocytes in that tissue, but some inherent tendency toward more stable gene expression in the
326 UON after injury. Qu and Jakobs found that UON astrocyte genes and proteins generally were
327 downregulated, while microglial markers were upregulated after ON crush [13]. Interestingly, expression
328 of *Gfap* did not increase after crush in their work, nor in the present study in any region or model.
329 Increased GFAP protein is often regarded as key sign of "reactivity" in the brain, where it normally is
330 expressed at low levels, only increasing after pathological insults. In contrast, *Gfap* is expressed at a high
331 level in naïve UON and does not further increase after crush or in rodent glaucoma models [14, 15, 38].

332 While prior research assumed that astrocyte "reactivity" was detrimental to neuronal survival,
333 the reactions of astrocytes to injury can be both beneficial and harmful [39-42]. A proposed paradigm
334 suggesting that there is an A1/A2 astrocyte dichotomy is now considered simplistic, and features of each
335 are found within the same cells. Astrocytes exhibit important local and age-related heterogeneity in
336 gene expression, structure, and function [43-47]. Our data show that the genes reported to be active in
337 detrimental (A1) and beneficial (A2) astrocyte responses in other models [48] are more prominently
338 expressed in the MON after crush and glaucoma, as well as in the crush model UON, than they are in
339 UON glaucoma. However, there was no clear pattern for differential upregulation of groups of genes
340 reported to be typical for A1 or A2 "phenotypes". Astrocytes have protective functions, and review of
341 astrocytic responses in retina suggests inhibiting some astrocyte responses could be neuroprotective
342 [39, 49-52]. Furthermore, beneficial astrocytic behavior is driven by the *Stat3* pathway, which can
343 worsen mouse glaucoma damage when genetically removed[39]. Experimental inflammation leads to

344 changes in single cell gene expression that produces many subtype-specific patterns in astrocytes in
345 particular brain regions [53].

346 Many genes known to be related to microglia changed in the both the MON and UON in the
347 glaucoma model. There are microglia in the ONH and have been shown to increase in number in rat
348 glaucoma models [54, 55]. Interestingly, mice lacking microglia still undergo neurodegeneration after
349 ON crush [56]. Microglia in the ON interact with astrocytes via complement 1q, tumor necrosis factor α,
350 and interleukin 1, activating some detrimental astrocytic behavior. Microglial knockout mice do not
351 develop detrimental astrocytic actions in brain. Microglia have been characterized into reactive forms
352 that are both pro-inflammatory (M1) and immunoregulatory (M2), though these may not be mutually
353 exclusive [47] and dichotomizing microglial responses may be oversimplistic as discussed in the context
354 of astrocytes. The activation of NF-kB in microglia is particularly associated with detrimental effects in
355 brain and glaucoma models of disease and microglial adenosine receptor activation, resulting from ATP
356 release from stressed astrocytes, may reduce microglial activation [57, 58].

357 Cellular pathways selectively active in UON included Wnt, Hippo, PI3K-Akt, and TGFβ signaling.
358 Their interactions are complex but are highly related to mechanosensation via transcellular membrane
359 mechanisms. Wnt signaling through cell membrane receptors activates both the Rho and Rac1
360 pathways, affecting the actin cytoskeleton [59]. In astrocytes, RhoA limits astrogliosis and anti-
361 regenerative action by suppressing Yes-activated protein signaling (the Hippo pathway) through actin-
362 mediated compaction, but independent of microtubules [60]. RhoA also affects the actin cytoskeleton
363 by activating Rho-kinase, inactivating cofilin and activating the actin motor myosin II [61]. Wnt signaling
364 also activates *Rac1*, and *Racgap1*, *Iqgap3*, and *Dock2* genes in this pathway that were upregulated in
365 three day glaucoma. Other genes that act through cell membrane receptors that were upregulated in
366 our glaucoma samples included thrombospondin, part of the TGFβ signaling system. The relationship of
367 membrane signaling through junctional complexes in astrocytes warrants additional focus.

368 Our study has several limitations of note. To study gene expression of cells in their native state
369 or resident within tissue under experimental conditions, we analyzed whole tissues and not cell type-
370 specific or single cells. Thus, we cannot distinguish that the significantly changed genes found in these
371 studies are exclusively produced by astrocytes or other cell types. In comparing the effects of glaucoma
372 and ON crush, we are aware that there was somewhat greater RGC damage in ON crush that could have
373 an unknown effect on our analysis when comparing the two models. In mammalian eyes with
374 connective tissues in the ONH, there are fibroblasts present in the extensive extracellular matrix. Gene
375 expression profiles have been done on cultured lamina cribrosa fibroblasts, whose behavior may lead to
376 different reactions in larger mammalian eyes than in mice that largely lack these cells [23].

377

378 **Conclusions**

379 Mouse UON tissue expresses genes that are distinct from immediately adjacent areas of the
380 retina and MON, as well as being nearly unique in the central nervous system. The major DEGs in UON
381 tissue were those likely to arise from the dominant astrocytes of this region and their extracellular
382 matrix and signaling through membrane receptors, along with pathways affecting cell response to
383 mechanostimulation. The responses to two different types of injury were more diverse in the MON than
384 in the UON, but included both stimulation and inhibition of cell proliferation in both regions. There was
385 no consistent gene expression pattern regarding typical astrocyte responses considered to be beneficial
386 or detrimental. Further analysis stemming from these data will include detailed dissection of the cell—
387 matrix interaction responses to experimental glaucoma.

388

389

390 **Materials and Methods**

391 *Animals*

392 Twenty four two to four month old C57BL/6 (B6, Cat # 0664, Jackson Laboratories, Bar Harbor,
393 ME, USA) mice were used for RNA-seq experiments (Table S2). An equal number of male and female
394 animals were included in all sample groups. For additional quantitative polymerase chain reaction
395 (qPCR) studies, tissue was obtained from three two to six month old bilateral naïve, wild-type, (non-
396 fluorescent) FVB/N-Tg(GFAP-GFP)14Mes female littermate mice (WT GFAP-GFP, Jackson Laboratories
397 #003257, Bar Harbor, ME, USA) as described in a previous publication[8] (Table S2).

398 *Anesthesia*

399 For surgical procedures and euthanasia, animals were anesthetized with an intraperitoneal
400 injection of 50 mg/kg ketamine (Fort Dodge Animal Health, Fort Dodge, IA), 10 mg/kg xylazine (VedCo
401 Inc., Saint Joseph, MO), and 2 mg/kg acepromazine (Phoenix Pharmaceuticals, Burlingame, CA), and
402 received topical ocular anesthesia of 0.5% proparacaine hydrochloride (Akorn Inc. Buffalo Grove, IL,
403 USA). For IOP measurements independent of additional procedures, animals were anesthetized using a
404 Rodent Circuit Controller (VetEquip, Inc., Pleasanton, CA, USA) delivering 2.5% isoflurane in oxygen at
405 500 cc/min.

406 *IOP Measurements*

407 IOP measurements were obtained using a TonoLab tonometer (TioLat, Inc., Helsinki, Finland),
408 recording the mean of six readings with optimal quality grading. IOP was first measured prior to the
409 procedure, and at one day, three days, one week, two weeks, and six weeks post-procedure until the
410 animal was sacrificed.

411 *Microbead Injections (Glaucoma Model)*

412 IOP elevation by microbead injection was performed in twelve B6 mice using a previously
413 established protocol [23]. IOP elevation was produced by unilateral anterior chamber microbead
414 injection. Erthoymycin ophthalmic ointment USP, 0.5% (Baush + Lomb, Laval, Canada) was given
415 bilaterally to prevent infection and lubricate the eye during recovery. The naïve eyes of treated animals
416 and both eyes of bilaterally naïve mice were used as controls in IOP analysis. Animals were sacrificed at
417 the following time points after injection for analysis: three days, two weeks, and six weeks. A total of
418 two males and two females were included for each time point.

419 *ON Crush*

420 Eight animals were subjected to unilateral ON crush. Topical proparacaine was used to numb
421 the eyes and 5% betadine was applied to disinfect prior to surgery. The conjunctiva was incised, and the
422 orbital venous sinus carefully dissected away to reveal the ON. The nerve was crushed for three seconds
423 using self-closing forceps (Dumoxel, World Precision Instruments, Sarasota, FL). Erythromycin
424 ophthalmic ointment USP, 0.5% (Baush + Lomb, Laval, Canada) was given bilaterally to prevent infection
425 and lubricate the eye during recovery. Animals were sacrificed at either three days or two weeks post-
426 crush for analysis (n = 2 males and 2 females per time point).

427 *Tissue Collection*

428 Three different tissue regions were dissected from each animal: UON, MON, and retina. Tissue
429 was collected from bilateral naïve animals for naïve control studies, as well as time points following
430 glaucoma/bead-injection and ON crush, on the same collection days. Animals were euthanized with
431 general intraperitoneal anesthesia as described above. The eyes were first enucleated and rinsed in cold
432 PBS, and the ON was cut flush to the globe. The dissected UON portions were ~200 µm in length
433 (calculated using digital calipers, and prior to the delineated opaque myelin transition zone), consistent
434 with a prior study [62]. The next 200–300 µm portion of nerve containing the myelin transition zone was

435 discarded. The MON collected was the first myelinated section posterior to the myelin transition zone,
436 200–300 µm in length. Next, the anterior chamber was excised, and retina was removed with little to no
437 retinal pigment epithelium/choroid attached. Dissected tissue was immediately placed into individual,
438 pre-chilled 1.5 mL Eppendorf tubes and flash frozen in liquid nitrogen before long-term storage at -80°C.
439 Tissue taken from naïve WT GFAP-GFP animals was immediately placed into QIAzol Lysis Reagent
440 (QIAgen) and processed using the manufacturer's protocol as previously reported [24]. For qPCR, both
441 right and left eyes from three animals were collected for each tissue region for a total of six replicates.

442 *Total RNA Extraction*

443 TRIzol® Reagent was added to each Eppendorf tube of frozen tissue immediately following
444 removal from storage. Volumes were adjusted for each tissue region based on approximate size/weight.
445 Tissue was homogenized at room temperature using a battery-operated, motorized pestle, and total
446 RNA was extracted according to the manufacturer's protocol.

447 *RNA-seq Library Preparation and Sequencing*

448 For the three tissue regions, male and female replicate RNA samples (n = 4 replicates per tissue
449 per treatment/time point, with n = 2 replicates of each sex) were pooled by sex for a total of 36
450 individual samples processed for RNA-seq. Pooled RNA was submitted to Genewiz (from Azenta Life
451 Sciences) for library preparation and sequencing. Sample quality control was performed prior to
452 generating the libraries. Libraries were prepared using an ultra-low input kit for paired-end sequencing
453 (2 x 150 bp) using an Illumina HiSeq instrument. On average, 40M reads were generated per sample
454 (Figure S8).

455

456 *RNA-seq Analysis*

457 Paired-end reads were aligned to the mouse reference genome (GRCm38) using HISAT2 (v2.2.1)
458 with default parameters [63]. FastQC was performed to assess overall sequence quality [64]. Next,
459 mapped reads were assembled into transcripts through StringTie (v1.3.0) [65]. Gene annotation
460 GRCm38 M25 from gencode was used. Expression from both reference and *de novo* transcripts were
461 reported.

462 To conduct differential gene expression analysis, a raw gene count table was prepared using the
463 'prepDE.py' script provided with StringTie. For each treatment and tissue, a DESeq2 model was fit to
464 compare each treatment time point to the control while accounting for sex.

465 $$\text{Expression} = \beta_1 \text{TREATMENT_TIME_POINT} + \beta_2 \text{SEX}$$

466 where TREATMENT_TIME_POINT = 0, 3 day, 2 week, 6 week. and SEX = FEMALE, MALE.

467 Differential genes comparing each treatment time point to control were reported separately.
468 Specifically, genes with a false discovery rate (FDR) < 0.05 and an absolute log2 fold change > 1 were
469 considered significantly differential genes.

470 To conduct principal component analysis (PCA), raw gene counts were first normalized into
471 FPKM (Fragments Per Kilobase of transcript per Million mapped reads) by adjusting for gene lengths.
472 Genes with FPKM < 1 in all samples were filtered out. Then, highly variable genes were selected. To
473 select highly variable genes, a mean-adjusted variance is computed for each gene. Mean and variance of
474 gene FPKM across all samples were first log10 transformed. Lowess regression was fit between
475 transformed variance and mean. Mean-adjusted variance for each gene was calculated by dividing its
476 variance by its predicted variance from the Lowess fit. By this procedure, 2633 genes with mean-

477 adjusted variance larger than 1.5 were selected. Finally, to conduct PCA, FPKM for each gene was
478 standardized and 'prcomp' was applied to compute the top two principal components.

479 KEGG pathway analysis for significantly changed genes was completed using g:Profiler GOst
480 (Version: 0.1.7) [66] with the multiple testing correction method applying a significance threshold of
481 0.05. Sample distances were measured by log2 transformation of the normalized counts data and
482 calculation of the Euclidean distance between samples.

483 *Quantitative Polymerase Chain Reaction (qPCR)*

484 cDNA was synthesized from purified RNA using the High-Capacity Reverse Transcription Kit
485 (Thermo Fisher) per the manufacturer's instructions. SsoAdvanced Universal SYBR Green Supermix (Bio-
486 Rad) was used for qPCR with exon junction-spanning primers (Table S3). Primer efficiencies were
487 checked and melt curve analyses were performed prior to experimental use of all primer pairs included
488 in this study. Data was analyzed using the Delta Ct method (plotted as relative expression), where the
489 triplicate raw Ct values were first averaged, then normalized to the geometric mean of three
490 housekeeping genes (Table S3). The mean of the six samples from three biological replicates were
491 plotted for each tissue analyzed.

492 **Figures and Tables with Captions**

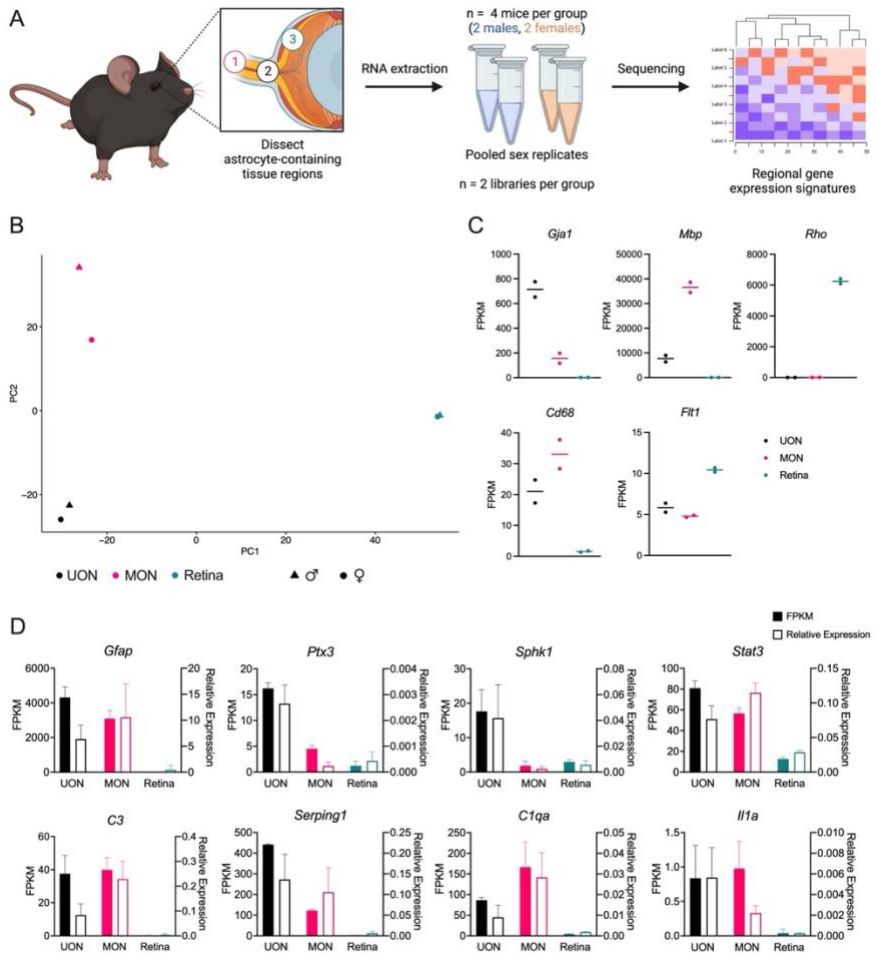

493

494 **Figure 1.** Transcriptomic analysis of astrocyte-containing tissues in bilaterally naïve mice. **(A)**
495 Experimental design of the study. Three tissue regions of bilaterally naïve mice were micro-dissected for
496 comparison: 1) myelinated optic nerve (MON), 2) unmyelinated optic nerve (UON), and 3) retina. Tissue
497 from four mice were collected and the sex replicates for each tissue group were pooled after RNA
498 extraction for library preparation and 150 bp paired end Illumina sequencing. **(B)** Principal component
499 analysis (PCA) of bilaterally naïve tissue regions. Each symbol represents a single sample, where symbol
500 colors denote the tissue region and symbol shapes signify sex. **(C)** FPKM (Fragments Per Kilobase of
501 transcript per Million mapped reads) expression of cell type markers characteristic of each tissue region:
502 glial (*Gja1*, encodes for Connexin-43), oligodendrocyte (*Mbp*, encodes for myelin basic protein), retinal

503 (*Rho*, encodes for Rhodopsin), microglial (*Cd68*, encodes for Cluster of Differentiation 68), and
504 capillary/endothelial (*Flt1*, encodes for VEGFR1). Dots represent a single sample and lines represent the
505 median FPKM of the replicate samples. **(D)** Expression of astrocyte genes in three naïve tissue regions:
506 UON, MON, and retina. Left y-axis and filled bars represent FPKM (from RNA-seq data), while right y-axis
507 and empty bars indicate relative expression via qPCR of independent tissue samples. Error bars indicate
508 standard deviation. For RNA-seq, n = 2 (pooled) samples per tissue type. For qPCR, n = 6 samples from 3
509 mice per tissue group.

510

511

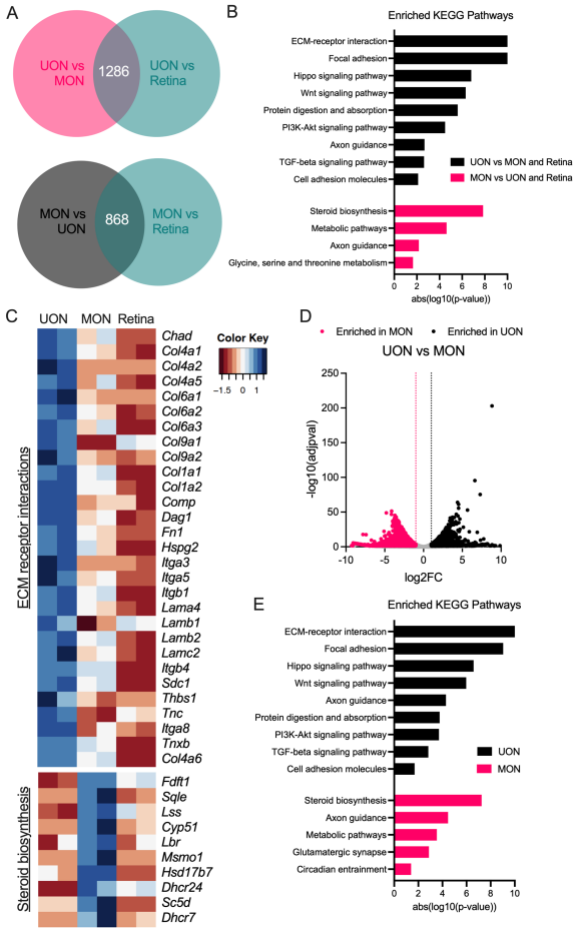

Figure 2. Region-specific gene signatures in the naïve ON. **(A)** Venn diagrams showing the number of significantly enriched genes in naïve UON compared to MON and retina (top) and MON compared to UON and retina (bottom). **(B)** KEGG analysis of enriched UON (top) and MON (bottom) genes compared to all other tissue regions. **(C)** Clustered heatmaps of significantly upregulated UON genes within the extracellular matrix (ECM)–receptor interactions (top) and MON-enriched genes in the steroid biosynthesis (bottom) KEGG pathways. **(D)** Volcano plot showing differential expression analysis comparing naïve UON and MON. Dotted lines indicate threshold cut-off for a significantly changed gene ($\log_2FC \pm 1$, in addition to adjusted $p < 0.05$). Genes with $\log_2FC > 1$ were considered enriched in UON, and genes with $\log_2FC < -1$ signified MON-enriched genes. **(E)** KEGG pathways enriched in UON and MON genes.

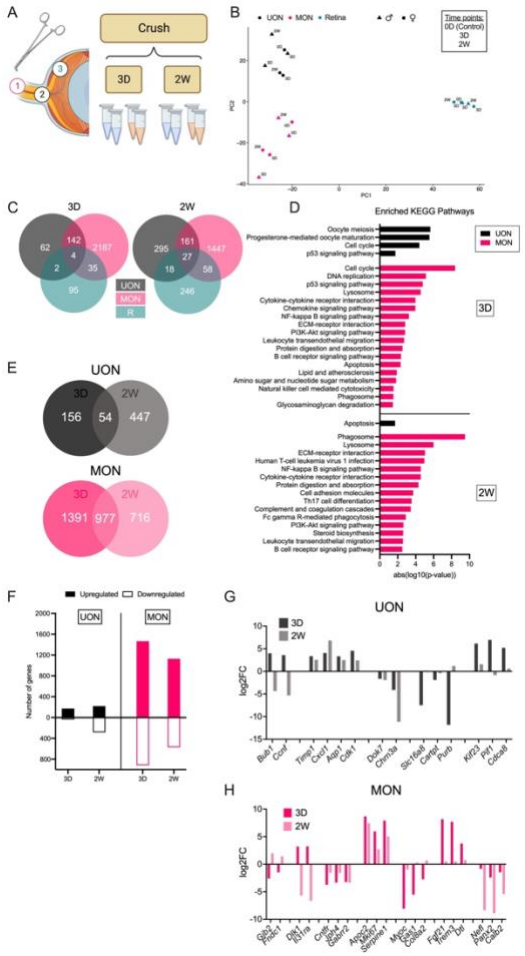

Figure 3. Differential responses to ON crush. **(A)** Experimental design for studying gene expression responses following ON crush in UON, MON, and retinal tissue. **(B)** PCA of tissue during the ON crush time course. **(C)** Venn diagrams showing relationships of differentially expressed genes (DEGs) between UON, MON, and retina three days (left, 3D) and two weeks (right, 2W) after crush. **(D)** KEGG pathway analysis of UON and MON DEGs at early (top) and late (bottom) crush time points. **(E)** Venn diagrams showing relationships of UON (top) and MON (bottom) responses to ON crush. **(F)** Number of upregulated and downregulated genes in UON and MON at each crush time point. **(G-H)** Gene expression changes in UON (G) and MON (H) during the ON crush time course.

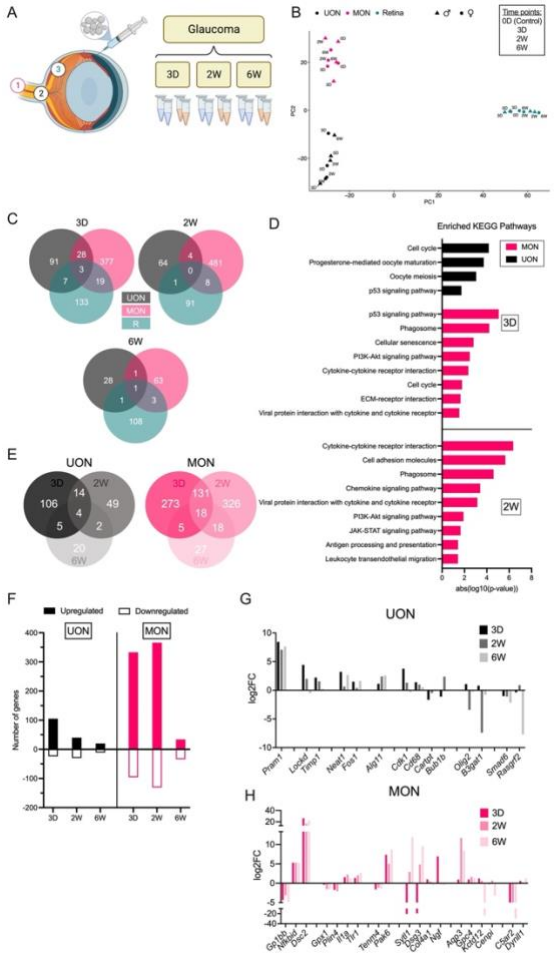

Figure 4. Differential responses to glaucoma. **(A)** Experimental design for RNA-seq experiments in the bead-induced glaucoma model. **(B)** PCA of control and experimental glaucoma tissue time points. **(C)** Venn diagrams showing relationships of DEGs between UON, MON, and retina three days, two weeks, and six weeks after IOP elevation. **(D)** KEGG pathway analysis of UON and MON DEGs at different time points following IOP elevation. **(E)** Venn diagrams showing relationships of UON (left) and MON (right) responses to bead-induced glaucoma. **(F)** Number of up/down genes in UON and MON at each glaucoma time point. **(G-H)** Gene expression changes in UON (G) and MON (H) during the glaucoma time course.

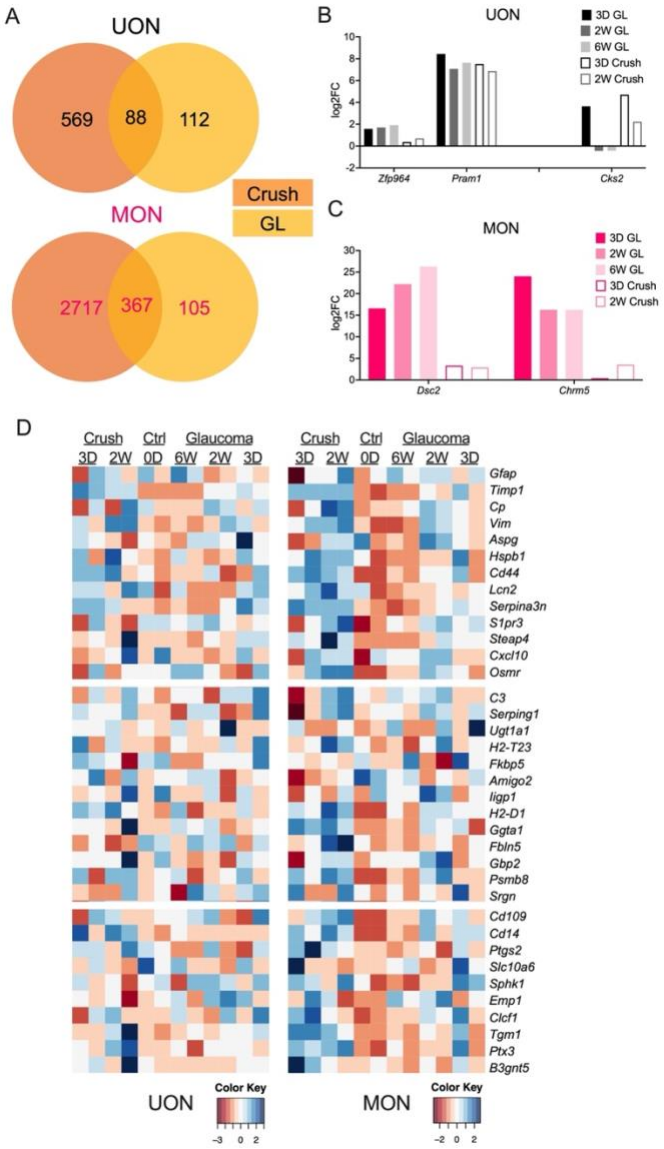

Figure 5. Shared responses to ON injury. **(A)** Venn diagrams comparing DEGs in ON crush and glaucoma injuries in UON (top) and MON (bottom) tissue regions. DEGs are both upregulated and downregulated in at least one time point. **(B-C)** Gene expression of select UON (B) and MON (C) DEGs in ON crush and glaucoma injury. **(D)** Heatmap showing PAN-reactive, A1-specific, and A2-specific astrocyte markers in naïve and injured UON and MON regions. UON tissue did not express a dominant A1 or A2 characteristic phenotype in crush or glaucoma, while MON exhibited slightly more consistent A1/A2-specific gene expression compared to UON tissue.

551

552 **Supplementary Materials**

553 Figures S1-8

554 Figure S1: qPCR validation of naïve RNA-seq data.

555 Figure S2: Gene signature of the naïve mouse retina.

556 Figure S3: Expression of RGC marker genes in retinal tissue following ON injury.

557 Figure S4: IOP measurements over time in the microbead-induced glaucoma model.

558 Figure S5: Sex-specific gene expression differences in disease models.

559 Figure S6: Differential responses to crush and glaucoma in the retina.

560 Figure S7: A1/A2-specific gene signatures in the retina.

561 Figure S8: Total number of sequences.

562

563 Tables S1-3

564 Table S1: IOP measurements over time in the microbead-induced glaucoma model.

565 Table S2: Animals used in this study.

566 Table S3: qPCR primers used in this study.

567

568 Spreadsheets S1-5

569 Spreadsheet S1: List of DEGs and their relationships between all tissue regions in ON crush.

570 Spreadsheet S2: List of DEGs and their relationships between all tissue regions in the glaucoma model.

571 Spreadsheet S3: List of UON DEGs by time point in ON crush and glaucoma models.

572 Spreadsheet S4: List of MON DEGs by time point in ON crush and glaucoma models.

573 Spreadsheet S5: List of retina DEGs by time point in ON crush and glaucoma models.

574 Spreadsheet S6: List of DEGs comparing disease models by tissue region.

575

576 **Funding Information**

577 This study was supported in part by PHS research grants EY 02120 (HAQ) and 5P30EY001765
578 (Wilmer Eye Institute Core grant), NIH grant R01HG009518 (HJ), the A. Edward Maumenee Professorship
579 (HAQ), and unrestricted support from Mary Bartkus and from Tom Forrester.

580 **Acknowledgements**

581 Schematics for Figures 1, 3, and 4 were created with BioRender.com.

582 **Author Contributions**

583 HAQ conceptualized ideas, wrote and edited the manuscript, and acquired funding. CJK
584 performed tissue preparations, analyzed study data, and wrote and edited the manuscript. TVJ provided
585 concepts and experimental advice, carried out animal treatment, and edited the manuscript. DJZ
586 provided concepts and experimental advice and edited the manuscript. MW, WF, and HJ performed
587 bioinformatic analysis. SQ, EK and JS carried out animal treatment and tissue preparation. All authors
588 read and approved the final manuscript.

589 **Conflicts of Interest**

590 The authors declare no conflict of interests.

591 **Institutional Review Board Statement**

592 All animal protocols were in accordance with the guidelines of the ARVO Statement for the Use
593 of Animals in Ophthalmic and Vision Research and approved and monitored by the Johns Hopkins
594 University School of Medicine Animal Care and Use Committee (Protocol #MO21M401).

595 **Data Availability Statement**

The dataset supporting the conclusion of this article is available in the [repository name] repository, [unique persistent identifier and hyperlink to dataset in http:// format] and included within the article (and its additional files).

599 **REFERENCES**

600

601 1. Boland, M.V. and H.A. Quigley, *Risk factors and open-angle glaucoma: classification and*

602 *application.* J Glaucoma, 2007. **16**(4): p. 406-18.

603 2. Morrison, J.C., et al., *Understanding mechanisms of pressure-induced optic nerve damage.* Prog

604 Retin Eye Res, 2005. **24**(2): p. 217-40.

605 3. Howell, G.R., et al., *Axons of retinal ganglion cells are insulted in the optic nerve early in DBA/2J*

606 *glaucoma.* J Cell Biol, 2007. **179**(7): p. 1523-37.

607 4. Quigley, H.A., et al., *Optic nerve damage in human glaucoma. II. The site of injury and*

608 *susceptibility to damage.* Arch Ophthalmol, 1981. **99**(4): p. 635-49.

609 5. Sun, D., et al., *The morphology and spatial arrangement of astrocytes in the optic nerve head of*

610 *the mouse.* J Comp Neurol, 2009. **516**(1): p. 1-19.

611 6. Downs, J.C., M.D. Roberts, and C.F. Burgoyne, *Mechanical environment of the optic nerve head*

612 *in glaucoma.* Optom Vis Sci, 2008. **85**(6): p. 425-35.

613 7. Kobayashi, S., et al., *Expression of neural cell adhesion molecule (NCAM) characterizes a*

614 *subpopulation of type 1 astrocytes in human optic nerve head.* Glia, 1997. **20**(3): p. 262-73.

615 8. Quillen, S., et al., *Astrocyte responses to experimental glaucoma in mouse optic nerve head.* PLoS

616 One, 2020. **15**(8): p. e0238104.

617 9. Morrison, J.C., *Integrins in the optic nerve head: potential roles in glaucomatous optic*

618 *neuropathy (an American Ophthalmological Society thesis).* Trans Am Ophthalmol Soc, 2006.

619 **104**: p. 453-77.

620 10. Forrest, S.L., et al., *Distribution Patterns of Astrocyte Populations in the Human Cortex.*

621 Neurochem Res, 2022.

622 11. Mazumder, A.G., et al., *Astrocyte heterogeneity within white matter tracts and a unique*

623 *subpopulation of optic nerve head astrocytes.* iScience, 2022. **25**(12): p. 105568.

624 12. Ahmed, F., et al., *Microarray analysis of changes in mRNA levels in the rat retina after*
625 *experimental elevation of intraocular pressure.* Invest Ophthalmol Vis Sci, 2004. **45**(4): p. 1247-
626 58.
627 13. Qu, J. and T.C. Jakobs, *The Time Course of Gene Expression during Reactive Gliosis in the Optic*
628 *Nerve.* PLoS One, 2013. **8**(6): p. e67094.
629 14. Johnson, E.C., et al., *Cell proliferation and interleukin-6-type cytokine signaling are implicated by*
630 *gene expression responses in early optic nerve head injury in rat glaucoma.* Invest Ophthalmol
631 Vis Sci, 2011. **52**(1): p. 504-18.
632 15. Johnson, E.C., et al., *Global changes in optic nerve head gene expression after exposure to*
633 *elevated intraocular pressure in a rat glaucoma model.* Invest Ophthalmol Vis Sci, 2007. **48**(7): p.
634 3161-77.
635 16. Guttenplan, K.A., et al., *Neurotoxic Reactive Astrocytes Drive Neuronal Death after Retinal Injury.*
636 Cell Rep, 2020. **31**(12): p. 107776.
637 17. Tezel, G., et al., *An astrocyte-specific proteomic approach to inflammatory responses in*
638 *experimental rat glaucoma.* Invest Ophthalmol Vis Sci, 2012. **53**(7): p. 4220-33.
639 18. Hu, X., et al., *Interplay between Muller cells and microglia aggravates retinal inflammatory*
640 *response in experimental glaucoma.* J Neuroinflammation, 2021. **18**(1): p. 303.
641 19. Sun, D., J. Qu, and T.C. Jakobs, *Reversible reactivity by optic nerve astrocytes.* Glia, 2013. **61**(8):
642 p. 1218-35.
643 20. Karasawa, K., et al., *Patterns of aquaporin expression in the canine eye.* Vet J, 2011. **190**(2): p.
644 e72-e77.
645 21. Yang, P., et al., *DNA microarray analysis of gene expression in human optic nerve head*
646 *astrocytes in response to hydrostatic pressure.* Physiol Genomics, 2004. **17**(2): p. 157-69.

647 22. Salvador-Silva, M., et al., *Responses and signaling pathways in human optic nerve head*
648 *astrocytes exposed to hydrostatic pressure in vitro.* Glia, 2004. **45**(4): p. 364-77.
649 23. Cone-Kimball, E., et al., *Scleral structural alterations associated with chronic experimental*
650 *intraocular pressure elevation in mice.* Mol Vis, 2013. **19**: p. 2023-39.
651 24. Kimball, E., et al., *The role of aquaporin-4 in optic nerve head astrocytes in experimental*
652 *glaucoma.* PLoS One, 2021. **16**(2): p. e0244123.
653 25. Ling, Y.T.T., et al., *Pressure-Induced Changes in Astrocyte GFAP, Actin, and Nuclear Morphology*
654 *in Mouse Optic Nerve.* Invest Ophthalmol Vis Sci, 2020. **61**(11): p. 14.
655 26. Paisley, C.E. and J.N. Kay, *Seeing stars: Development and function of retinal astrocytes.* Dev Biol,
656 2021. **478**: p. 144-154.
657 27. Kimball, E.C., et al., *Aquaporin 4 is not present in normal porcine and human lamina cribrosa.*
658 PLoS One, 2022. **17**(6): p. e0268541.
659 28. Khakh, B.S. and M.V. Sofroniew, *Diversity of astrocyte functions and phenotypes in neural*
660 *circuits.* Nat Neurosci, 2015. **18**(7): p. 942-52.
661 29. Westergard, T. and J.D. Rothstein, *Astrocyte Diversity: Current Insights and Future Directions.*
662 Neurochem Res, 2020. **45**(6): p. 1298-1305.
663 30. Endo, F., et al., *Molecular basis of astrocyte diversity and morphology across the CNS in health*
664 *and disease.* Science, 2022. **378**(6619): p. eadc9020.
665 31. Chumakov, P.M., *Function of the p53 gene: choice between life and death.* Biochemistry (Mosc),
666 2000. **65**(1): p. 28-40.
667 32. Hernandez Borrero, L.J. and W.S. El-Deiry, *Tumor suppressor p53: Biology, signaling pathways,*
668 *and therapeutic targeting.* Biochim Biophys Acta Rev Cancer, 2021. **1876**(1): p. 188556.
669 33. Stracquadanio, G., et al., *The importance of p53 pathway genetics in inherited and somatic*
670 *cancer genomes.* Nat Rev Cancer, 2016. **16**(4): p. 251-65.

671 34. Wiggs, J.L., et al., *The p53 codon 72 PRO/PRO genotype may be associated with initial central*
672 *visual field defects in caucasians with primary open angle glaucoma.* PLoS One, 2012. **7**(9): p.
673 e45613.
674 35. Asefa, N.G., et al., *Bioinformatic Prioritization and Functional Annotation of GWAS-Based*
675 *Candidate Genes for Primary Open-Angle Glaucoma.* Genes (Basel), 2022. **13**(6).
676 36. Son, J.L., et al., *Glaucomatous optic nerve injury involves early astrocyte reactivity and late*
677 *oligodendrocyte loss.* Glia, 2010. **58**(7): p. 780-9.
678 37. Paralkar, V.R., et al., *Unlinking an lncRNA from Its Associated cis Element.* Mol Cell, 2016. **62**(1):
679 p. 104-10.
680 38. Howell, G.R., et al., *Molecular clustering identifies complement and endothelin induction as early*
681 *events in a mouse model of glaucoma.* J Clin Invest, 2011. **121**(4): p. 1429-44.
682 39. Sun, D., S. Moore, and T.C. Jakobs, *Optic nerve astrocyte reactivity protects function in*
683 *experimental glaucoma and other nerve injuries.* J Exp Med, 2017. **214**(5): p. 1411-1430.
684 40. Okada, S., et al., *Conditional ablation of Stat3 or Socs3 discloses a dual role for reactive*
685 *astrocytes after spinal cord injury.* Nat Med, 2006. **12**(7): p. 829-34.
686 41. Liddelow, S.A., et al., *Neurotoxic reactive astrocytes are induced by activated microglia.* Nature,
687 2017. **541**(7638): p. 481-487.
688 42. Jin, J., et al., *Glial pathology and retinal neurotoxicity in the anterior visual pathway in*
689 *experimental autoimmune encephalomyelitis.* Acta Neuropathol Commun, 2019. **7**(1): p. 125.
690 43. Lanjakornsiripan, D., et al., *Layer-specific morphological and molecular differences in neocortical*
691 *astrocytes and their dependence on neuronal layers.* Nat Commun, 2018. **9**(1): p. 1623.
692 44. Khakh, B.S. and B. Deneen, *The Emerging Nature of Astrocyte Diversity.* Annu Rev Neurosci,
693 2019. **42**: p. 187-207.

694 45. Chai, H., et al., *Neural Circuit-Specialized Astrocytes: Transcriptomic, Proteomic, Morphological,*
695 *and Functional Evidence.* Neuron, 2017. **95**(3): p. 531-549 e9.
696 46. Batiuk, M.Y., et al., *Identification of region-specific astrocyte subtypes at single cell resolution.*
697 Nat Commun, 2020. **11**(1): p. 1220.
698 47. Hinkle, J.T., V.L. Dawson, and T.M. Dawson, *The A1 astrocyte paradigm: New avenues for*
699 *pharmacological intervention in neurodegeneration.* Mov Disord, 2019. **34**(7): p. 959-969.
700 48. Zamanian, J.L., et al., *Genomic analysis of reactive astrogliosis.* J Neurosci, 2012. **32**(18): p. 6391-
701 410.
702 49. Cuenca, N., et al., *Cellular responses following retinal injuries and therapeutic approaches for*
703 *neurodegenerative diseases.* Prog Retin Eye Res, 2014. **43**: p. 17-75.
704 50. Cui, Q.N., et al., *The role of glia in the physiology and pharmacology of glucagon-like peptide-1:*
705 *implications for obesity, diabetes, neurodegeneration and glaucoma.* Br J Pharmacol, 2022.
706 **179**(4): p. 715-726.
707 51. Gharagozloo, M., et al., *Complement component 3 from astrocytes mediates retinal ganglion cell*
708 *loss during neuroinflammation.* Acta Neuropathol, 2021. **142**(5): p. 899-915.
709 52. Guttenplan, K.A., et al., *Neurotoxic reactive astrocytes induce cell death via saturated lipids.*
710 Nature, 2021. **599**(7883): p. 102-107.
711 53. Hasel, P., et al., *Neuroinflammatory astrocyte subtypes in the mouse brain.* Nat Neurosci, 2021.
712 **24**(10): p. 1475-1487.
713 54. Neufeld, A.H., *Microglia in the optic nerve head and the region of parapapillary chorioretinal*
714 *atrophy in glaucoma.* Arch Ophthalmol, 1999. **117**(8): p. 1050-6.
715 55. Bordone, M.P., et al., *Involvement of microglia in early axoglial alterations of the optic nerve*
716 *induced by experimental glaucoma.* J Neurochem, 2017. **142**(2): p. 323-337.

717 56. Hilla, A.M., H. Diekmann, and D. Fischer, *Microglia Are Irrelevant for Neuronal Degeneration and*
718 *Axon Regeneration after Acute Injury.* J Neurosci, 2017. **37**(25): p. 6113-6124.
719 57. Yang, X., et al., *Transgenic inhibition of astroglial NF-kappaB restrains the neuroinflammatory*
720 *and neurodegenerative outcomes of experimental mouse glaucoma.* J Neuroinflammation, 2020.
721 **17**(1): p. 252.
722 58. Ferreira-Silva, J., et al., *Activation of Adenosine A(3) Receptor Inhibits Microglia Reactivity*
723 *Elicited by Elevated Pressure.* Int J Mol Sci, 2020. **21**(19).
724 59. Ohnishi, M., et al., *Selective enhancement of wnt4 expression by cyclic AMP-associated*
725 *cooperation between rat central astrocytes and microglia.* Biochem Biophys Res Commun, 2015.
726 **467**(2): p. 367-72.
727 60. Hoffman, B.D., C. Grashoff, and M.A. Schwartz, *Dynamic molecular processes mediate cellular*
728 *mechanotransduction.* Nature, 2011. **475**(7356): p. 316-23.
729 61. Martino, F., et al., *Cellular Mechanotransduction: From Tension to Function.* Front Physiol, 2018.
730 **9**: p. 824.
731 62. Korneva, A., et al., *A method to quantify regional axonal transport blockade at the optic nerve*
732 *head after short term intraocular pressure elevation in mice.* Exp Eye Res, 2020. **196**: p. 108035.
733 63. Kim, D., et al., *Graph-based genome alignment and genotyping with HISAT2 and HISAT-*
734 *genotype.* Nat Biotechnol, 2019. **37**(8): p. 907-915.
735 64. de Sena Brandine, G. and A.D. Smith, *Falco: high-speed FastQC emulation for quality control of*
736 *sequencing data.* F1000Res, 2019. **8**: p. 1874.
737 65. Pertea, M., et al., *StringTie enables improved reconstruction of a transcriptome from RNA-seq*
738 *reads.* Nat Biotechnol, 2015. **33**(3): p. 290-5.
739 66. Raudvere, U., et al., *g:Profiler: a web server for functional enrichment analysis and conversions*
740 *of gene lists (2019 update).* Nucleic Acids Res, 2019. **47**(W1): p. W191-W198.

741